ADVANCED MATERIALS TECHNOLOGIES
www.advmattechnol.de

Hybrid Nanogenerator for Biomechanical Energy Harvesting, Motion State Detection, and Pulse Sensing

Minxing Du, Yu Cao, Xuecheng Qu, Jiangtao Xue, Weiyi Zhang, Xiong Pu, Bojing Shi, and Zhou Li**

Harvesting biomechanical energy to power wearable electronic devices shows great potential in the field of the Internet of Things. An insole hybrid nanogenerator (IHN) has been designed based on a combination of multilayered triboelectric nanogenerator and arched piezoelectric nanogenerator. The IHN not only can convert the mechanical energy of the footsteps into electricity, but also distinguishes three kinds of motion states: walking, stepping, and jumping. A maximum open-circuit voltage of 150 V and a short-circuit current of 4.5 µA are achieved from human body motions. After walking for 8 min, the IHN can charge a 100 µF capacitor to 2.5 V. Then, a self-powered dorsalis pedis artery monitoring system is designed, which can detect the pulse signals of the dorsalis pedis artery in real-time. The integrated design of energy collection, storage, and utilization has important application potential in future self-powered monitoring of patients and intelligent analysis of blood supply to the lower limbs in a professional athlete.

1. Introduction

The development of the Internet of Things technology puts forward higher requirements for wearable electronic devices.[1] Most of these devices are powered by batteries that are required to recharge and have a limited lifespan.[2] Human movements such as walking and running contain abundant available biomechanical energy. To prolong the using time of wearable electronic devices, some methods of converting biomechanical energy into electricity have become a hot research topic.[3] Three main methods of it have been reported: electromagnetic,[4] piezoelectric,[5] and triboelectric.[6] The electromagnetic generator converts biomechanical energy into electricity based on the law of electromagnetic induction.[7] The electromagnetic generator relies on rigid magnets and coils, which are usually not suitable for wearing. Piezoelectric nanogenerator (PENG) utilizes the piezoelectric effect of functional materials to convert biomechanical energy into electricity.[8] With the continuous development of materials science, the types of piezoelectric materials have become diversified. At present, about 200 types of piezoelectric materials have been reported for energy harvesting.[9] Among them, piezoelectric polymer and polymer composite materials[10] are widely used in wearable electronic devices because of their good mechanical flexibility and high strain resistance. In addition, triboelectric nanogenerator (TENG) has entered the horizon of researchers due to its many advantages such as strong structural adaptability, easy processing, and low cost.[11] Biological movement promotes the contact and separation of the triboelectric layer materials, which is accompanied by the triboelectric effect and electrostatic induction. The coupling of the two effects induces electrons to transfer between the back electrodes, which realize energy conversion. This technology has been used as active sensors[12] and energy harvesters.[13] At present, a large of cases of reliance on TENG to harvest biomechanical energy have been reported, such as joint activity,[14] muscle movement,[15] kinetic energy during body movement,[3c,16] heartbeat,[5c,17] breathing,[18] and blood flow.[19]

In this work, we introduce an insole hybrid nanogenerator (IHN) based on TENG and PENG. The parts of the forefoot and hindfoot are respectively composed of a sandwich structure

M. Du, X. Pu
School of Resources, Environment and Materials
Center on Nanoenergy Research
Guangxi University
Nanning 530004, China
Y. Cao, Z. Li
School of Physical Science and Technology
Center on Nanoenergy Research
Guangxi University
Nanning 530004, China
E-mail: zli@binn.cas.cn
X. Qu, J. Xue, W. Zhang, X. Pu, Z. Li
CAS Center for Excellence in Nanoscience
Beijing Key Laboratory of Micro-Nano Energy and Sensor
Beijing Institute of Nanoenergy and Nanosystems
Chinese Academy of Sciences
Beijing 101400, China
B. Shi
Beijing Advanced Innovation Centre for Biomedical Engineering
Key Laboratory for Biomechanics and Mechanobiology of Ministry of Education
School of Biological Science and Medical Engineering
Beihang University
Beijing 100191, China
E-mail: bjshi@buaa.edu.cn

The ORCID identification number(s) for the author(s) of this article can be found under https://doi.org/10.1002/admt.202101332.

DOI: 10.1002/admt.202101332

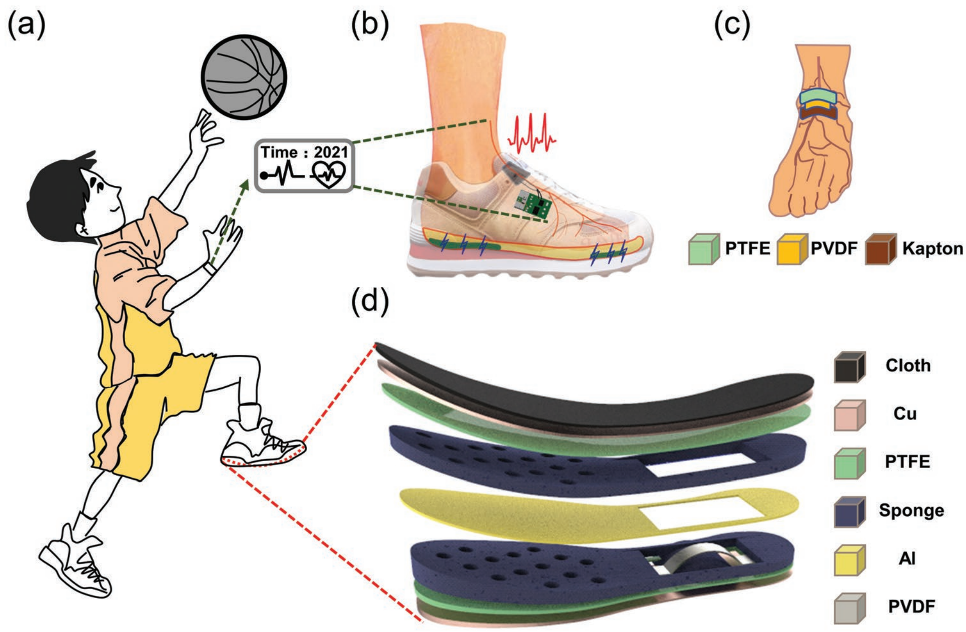

Figure 1. Overview diagram of the SAMS. a) Application diagram of the SAMS. b) Dorsalis pedis artery detection sensor system c) Structure diagram of dorsalis pedis artery signal acquisition device. d) Structure diagram of the IHN.

TENG and an arched PENG. The subtle method makes the two nanogenerators work well together and is used to analyze multiple gait types and collect biomechanical energy regardless of walking, stepping, and jumping. The stable energy output and excellent durability prove the ability of IHN to harvest biomechanical energy of feet as a wearable electronic device. Meanwhile, we developed a self-powered dorsalis pedis artery monitoring system based on the IHN, which reveals great potential in the fields of biosensor systems for medicine and sports in the future.

2. Results and Discussion

2.1. Structure and Working Principle of IHN and SAMS

The SAMS main includes an IHN sensor, a dorsalis pedis artery sensor, and an integrated processor module (**Figure 1**a). The processor module is fixed on the outside of the shoe, the dorsalis pedis artery sensor is located inside the "tongue" of the shoe, and the wire is transmitted through the shoe hole (Figure 1b). The dorsalis pedis artery sensor is made by a PVDF film packaged by PTFE and Kapton layers (Figure 1c). The PVDF film converts the vibration signal of the pulse into an electrical signal effectively. The encapsulation layers guarantee the durability and stability of the sensor. The forefoot of the IHN is a sandwich structure TENG, and the hindfoot is an arched PENG (Figure 1d; Figure S1a, Supporting Information). Various through-holes with a diameter of 2 cm are made on the forefoot of the sponge insole. The three triboelectric layers (PTFE-Al-PTFE) are separated by two sponge layers with through-holes (Figure S1a, Supporting Information). When the foot falls and rises, the Al layer and the PTFE layers are contacted and separated in the through-hole of the sponge. The Cu electrode on the back of PTFE acts as a source of transferred charge through electrostatic induction, and the Al layer is used as both a triboelectric layer and an electrode. The TENG with a sandwich structure is embedded in the insole, which could not only satisfy the comfort of wearing, but also improve the output by increasing the number of generators in parallel.[20] A rectangle with a size of 2 cm × 7 cm is removed from the hindfoot of the sponge insole, where embedded an arched PENG. The PENG is made of a PVDF film, which is encapsulated by an arched Kapton and a PE film (Figure S1b, Supporting Information). The design of this arch structure increases the shape variable of PVDF piezoelectric material and improves the output performance of PENG.[21] Additionally, the IHN is easily prepared to have the same appearance and size as standard insoles, making it a substitute for daily use (Figure S1c,d, Supporting Information). Besides, a PE film and a cotton cloth were used to encapsulate the device to prevent the influence of sweat on the output of the IHN. As a result, it is very convenient to disassemble for cleaning or replace with new packaging alternatives. Meanwhile, the user could also use IHN as an independent substrate material and place other antibacterial and dehumidifying insoles on it. The support of the sponge and the packaging structure ensures that the IHN has both flexibility and a certain toughness. As shown in Figure S1e (Supporting Information), the IHN can adapt to a variety of external deformations and recovery, such as twisting, dragging, and bending. The subtle structure guarantees its ability to stably harvest movement energy in daily sports, such as walking, jumping, and running.

The working principle of the IHN is shown in **Figure 2**. Under the vertical pressure of the heel during walking, the arched PENG changes from an arch to a plane, resulting in a potential difference between the two electrodes of the PENG (Figure 2a).[22] With the forefoot falling on the ground, a contact

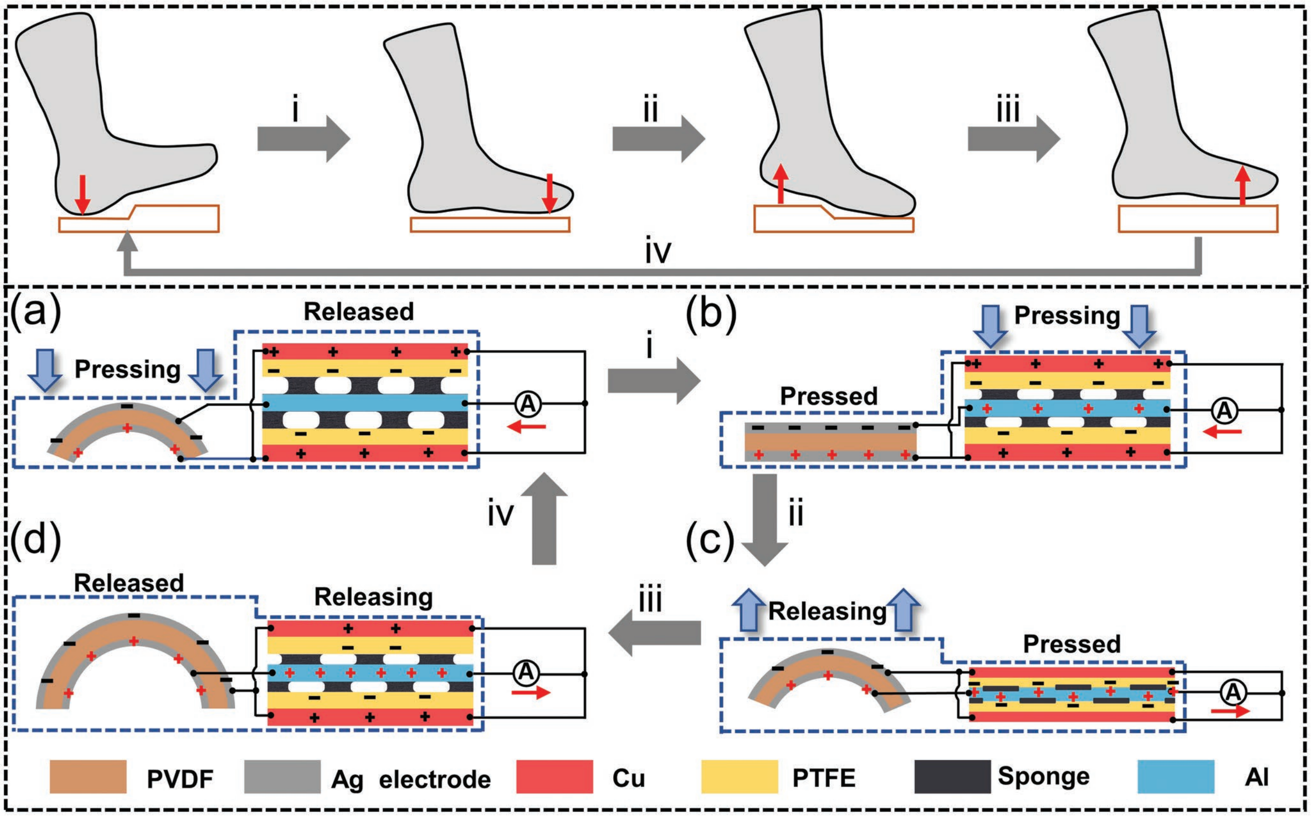

Figure 2. Working principle diagram of IHN in one walking cycle. The schematic diagram of the electronic flow process is accompanied by a) the hindfoot falling, b) the forefoot falling, c) the hindfoot raising, and d) the forefoot raising, respectively.

between PTFE and Al occurred in the through-hole of the sponge. As the pressure of the forefoot increases, the effective contact area between PTFE and Al increases. Due to the difference in electronegativity between PTFE and Al, the surface charge transfer between the two materials after contact induces a potential difference in the back electrode.[23] In the external circuit, electrons are driven by the potential difference to flow from the Cu electrode of the PTFE to the Al electrode (Figure 2b). When the heel is lifted, the PENG returns to the arch state due to the resilience of the sponge, which produces a current that is opposite to that when the hindfoot falls (Figure 2c). Finally, the forefoot is lifted, the PTFE layer and Al electrode in the TENG change from contact to separation. The charge on the Al electrode flows back to the Cu electrode in the external circuit, which is opposite to the current direction when the forefoot falls (Figure 2d). In one cycle of walking, the above four states occur in sequence. The parallel design of TENG and PENG makes the electron flow direction of the two devices the same, which makes the composite signal output of the IHN not lower than any one of them.

2.2. Electrical Performance of TENG, PENG, and IHN

To systematically study the contribution of TENG and PENG in the composite output, an experimenter with a weight of 600 N wears IHN for walking experiments. It is easy to find that there are four peaks in one cycle, which correspond to the four states of walking. (**Figure 3**a). When the hindfoot touches the ground, the voltage increased from 0 to 10 V. When the forefoot touches the ground, the voltage rises to 50 V. When the hindfoot is lifted, the voltage reversely changes to −10 V. When the forefoot is lifted, the voltage continues to transition in the reverse direction to about −50 V. This proves that the output signal of IHN can be used to characterize human gait information. To further verify the test results, the parallel interface between the two nanogenerators was disconnected, and the data of each was collected separately. Figure 3b,c shows the output waveforms of the TENG and the PENG after disconnection, and their respective characteristics are consistent with the waveforms in the composite output. Then, a COMSOL simulation was performed on the working state of PENG to compare the real situation in the experiment (Figure 3d,e), and the simulation results are consistent with the experimental results.

When we step and jump, the forefoot and hindfoot are raised and landed at the same time. PENG and TENG electrons flow in the same direction under the same force state. As described in Figure S2 (Supporting Information), we studied the output relationship between TENG and PENG in parallel. The value of the open-circuit voltage (V_{OC}) of the IHN is between that of the PENG and the TENG operating independently. Meanwhile, the short-circuit current (I_{SC}) and the transferred charges (Q_{SC}) present a superposition relationship. The PENG and the TENG of the IHN connected in parallel form an equivalent capacitance

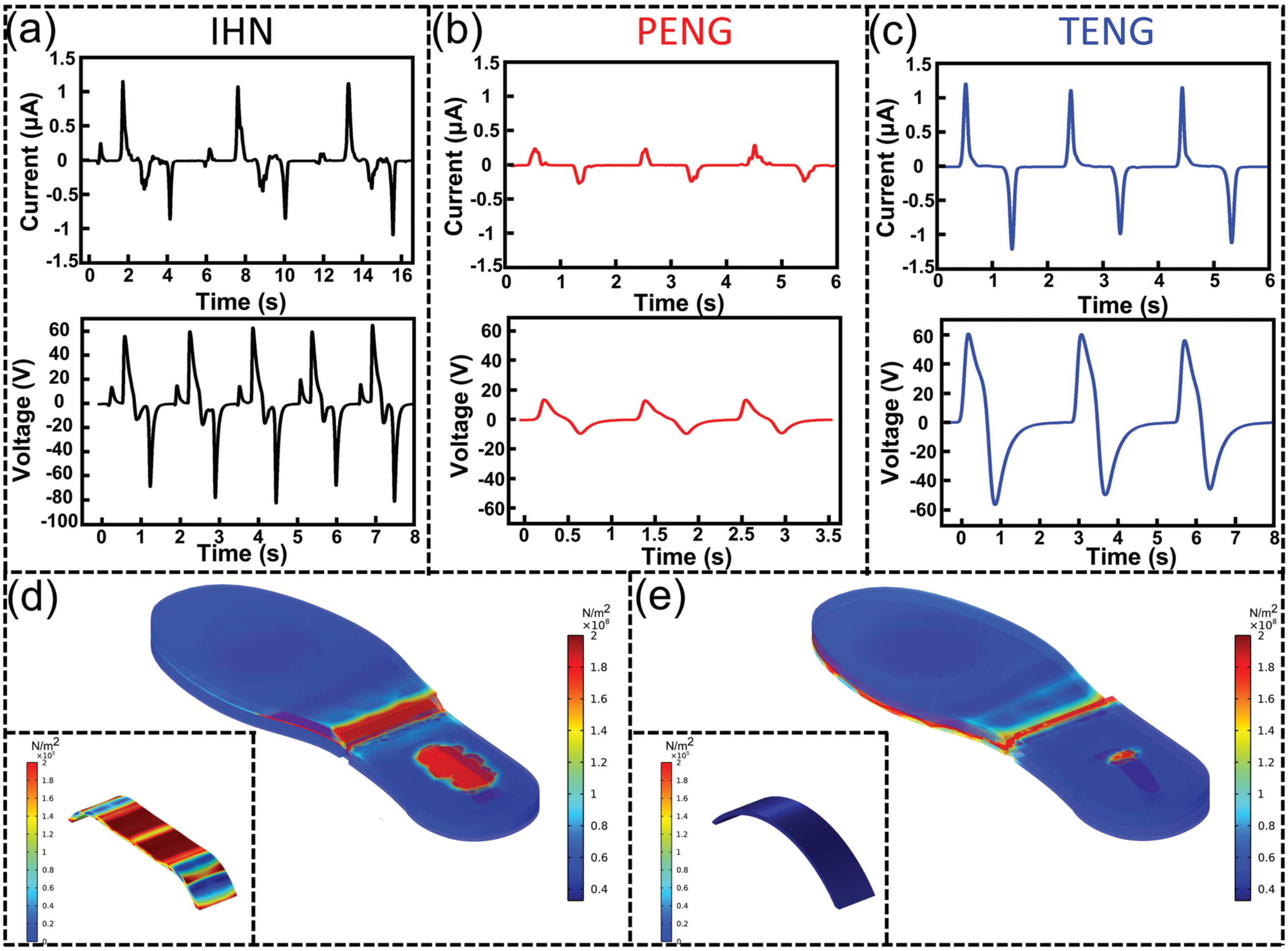

Figure 3. Outputs of IHN during walking. a–c) Short-circuit current I_{SC} and Open-circuit voltage V_{OC} of the IHN, the PENG, and the TENG, respectively. d) Stress and strain simulations of PENG when hindfoot dropped. e) Stress and strain simulations of PENG when hindfoot lifted.

model, which follows the basic rule of Maxwell's displacement current:[24]

$$J_D = \frac{\partial D}{\partial t} = \varepsilon_0 \frac{\partial E}{\partial t} + \frac{\partial P}{\partial t} \tag{1}$$

where J_D is the free electric current density, D is displacement field, ε_0 is permittivity in a vacuum, E is the electric field, and P is the polarization field. In conjunction with Ohm's law, we can establish the theories for different modes of IHN once it is connected with a load, regarding the power output:

$$Q_{SC} = CV_{OC} \tag{2}$$

$$I_{SC} = \Delta Q / \Delta t \tag{3}$$

where C is the equivalent capacitance of the IHN. The result is consistent with the capacitance model theory, which proves that the composite output performance of IHN is reliable. Based on this, the outputs of the IHN at different frequencies are measured to analyze the characteristics for daily use. The output of the device is collected under the conditions of 0.8–2.4 Hz to simulate the real gait, the bidirectional acceleration of linear motor corresponding to the frequency is 0.1, 0.5, 3.5, 8, and 42 m s^{-2}, respectively. The V_{OC} and the Q_{SC} were ≈120 V and 150 nC, respectively, and remained almost unchanged at various frequencies. However, the I_{SC} increases with frequency, rising from 1 μA at 0.8 Hz to 2 μA at 2.4 Hz (Figure S3, Supporting Information). The reason is the accumulated charge on the triboelectric layers of TENG reach gradually a saturated and stable state, and the amount of charge transferred in the process of each contact-separation is close to a constant value, which causes the induced potential difference of the back electrode to remain balanced. Meanwhile, the voltage and transferred charge of PENG are only related to the force. As a consequence, the composite voltage and charge of the IHN hardly change with frequency. As for the increase in current, this is because the increased contact and separation rate results in a fast flow rate of charges in the TENG, meanwhile, the faster frequency leads to a more frequent deformation of the PENG.

Further, the V_{OC}, the I_{SC}, and the Q_{SC} of the IHN pressed by a person weighing 600 N were measured when walking, stepping, and jumping (**Figure** 4a–c). In the test, the distance between the shoe and the ground was maintained at about

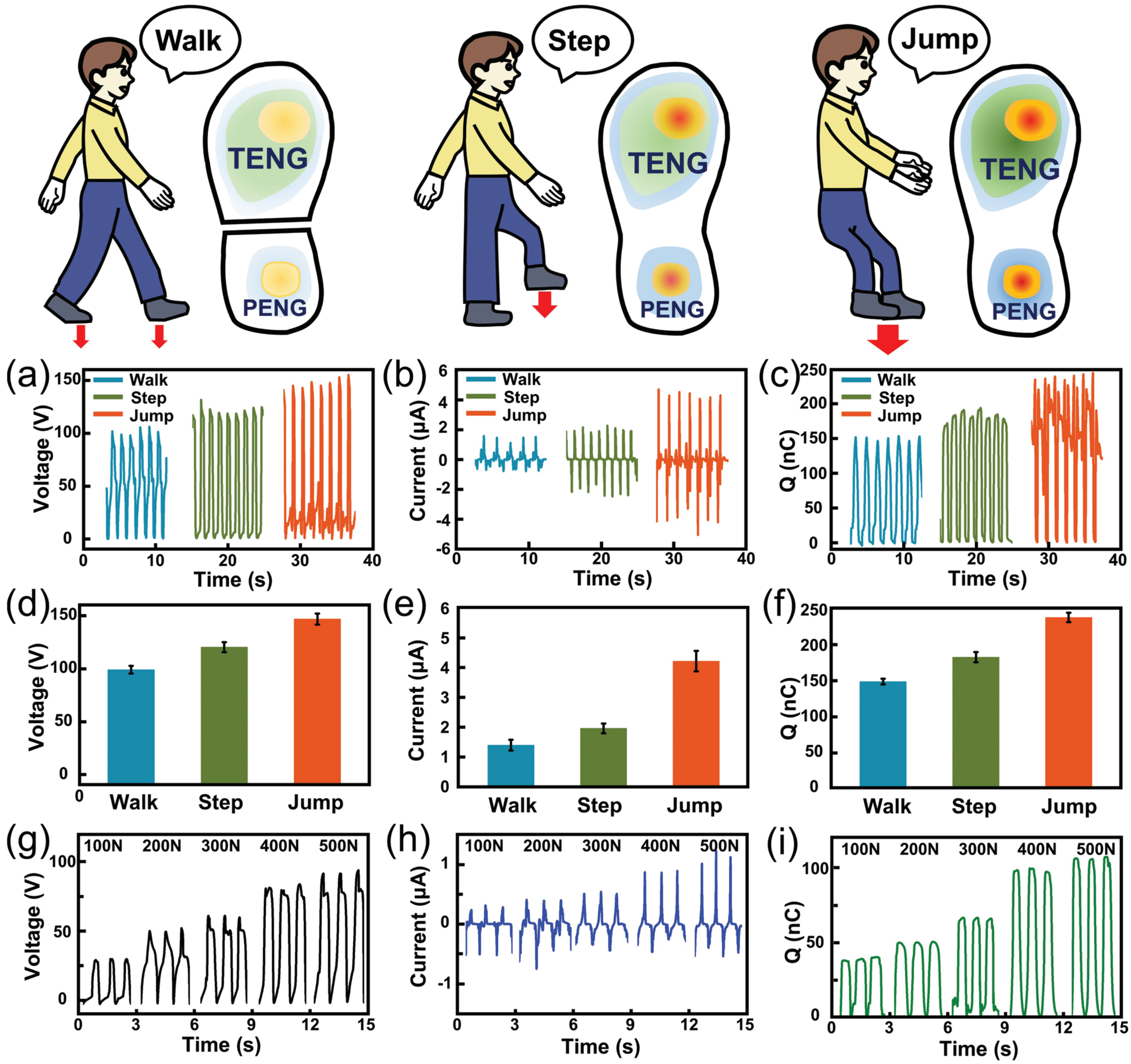

Figure 4. Gait analysis diagram of IHN. a–c) Comparison of V_{OC}, I_{SC}, and Q_{SC} of IHN in three gaits of walking, stepping, and jumping. d–f) Statistical results of peak values of V_{OC}, I_{SC}, and Q_{SC} of IHN during walking, stepping, and jumping. g–i) Comparisons of V_{OC}, I_{SC}, and Q_{SC} of IHN when stepping under different pressures.

5 cm while ensuring that the foot was close to the IHN. The PENG and the TENG work alternately when walking, and work simultaneously when stepping and jumping. It can be found that the voltage waveform of walking is significantly different from that of stepping and jumping. Besides, the output of jumping is larger than that of stepping and walking. It is because the instantaneous force when jumping to the ground is greater than stepping and walking, resulting in the largest effective contact area of the device. The maximum output can be obtained when jumping, the maximum open-circuit voltage can reach ≈150 V, the maximum short-circuit current can reach ≈4.5 μA, and the amount of charge can reach 240 nC. The researchers collected data for 20 action cycles every 1 min, performed ten times for each of the three gaits, and the output results were very stable (Figure 4d–f). Based on this, we studied the output of IHN under different pressures when stepping (Figure 4g–i). It can be found that the output voltage, current, and charge of IHN increase with the increase of pressure. Because with the increase of pressure, the contact area of TENG and the shape variable of PENG increase, and the number of transferred charge increases. When the INH is subjected to a pressure of 500 N, The maximum open-circuit voltage and short-circuit current of the IHN can reach 95 V and 1.2 μA.

Moreover, durability is an important condition that must be considered in the application. A 100 000-cycle fatigue test on IHN is carried out to verify the device quality, when the bidirectional acceleration of the motor is 1.5 m s^{-2} and the distance to press down is 5 mm. As shown in Figure S4a (Supporting Information), the measurement system consists of a linear motor with an acrylic plate, an oscilloscope, and an IHN. The peak to peak values of voltage, current, and transferred charge output are maintained at about 120 V, 2 µA, and 150 nC, respectively, which demonstrates that the device has decent durability and stability (Figure S4b, Supporting Information). This reliable performance shows that IHN as an energy harvester for portable electronic devices has very broad prospects in practical applications. The test environment and signal stability can be found in Video S1 (Supporting Information). Ulteriorly, to verify the output ability of IHN under bending deformation in actual use, bending fatigue tests were carried out on the forefoot part and hindfoot part, respectively. The experiment was performed at a bending angle of ≈30 degrees and a motor acceleration of 1.5 m s^{-2} for 10 000 cycles. As depicted in Figure S5 (Supporting Information), the output voltages of the two parts were stabilized at 10 and 5 V, respectively, and did not show significant attenuation. The decrease in voltage value is caused by the decrease in the active area, rather than the cause of the device itself. Therefore, this result shows that IHN is still reliable under extreme actions. The processes of bending fatigue test and data collection could be found in Video S2 (Supporting Information).

2.3. Application of IHN

To characterize the potential of IHN as a power supply in wearable electronic devices, here we have done IHN output test and power test under different loads when stepping (**Figure 5**a,b). It was found that a maximum power output of 77 µW can be obtained under a load of 40 MΩ. The IHN can charge a 100 µF capacitor to 2.5 V in 8 min during walking (Figure 5c). As a result, the IHN has a stable output capability and flexible structural design, which enables it to be easily adapted to a variety of portable energy supply strategies as a wearable power source. The IHN can be directly used to drive small electronic devices such as LED lights, meanwhile can be combined with energy storage circuits to collect energy as a backup (Figure 5d). The results show that 60 LED lights can be driven by the IHN directly (Figure 5e; Video S3, Supporting Information). Moreover, a

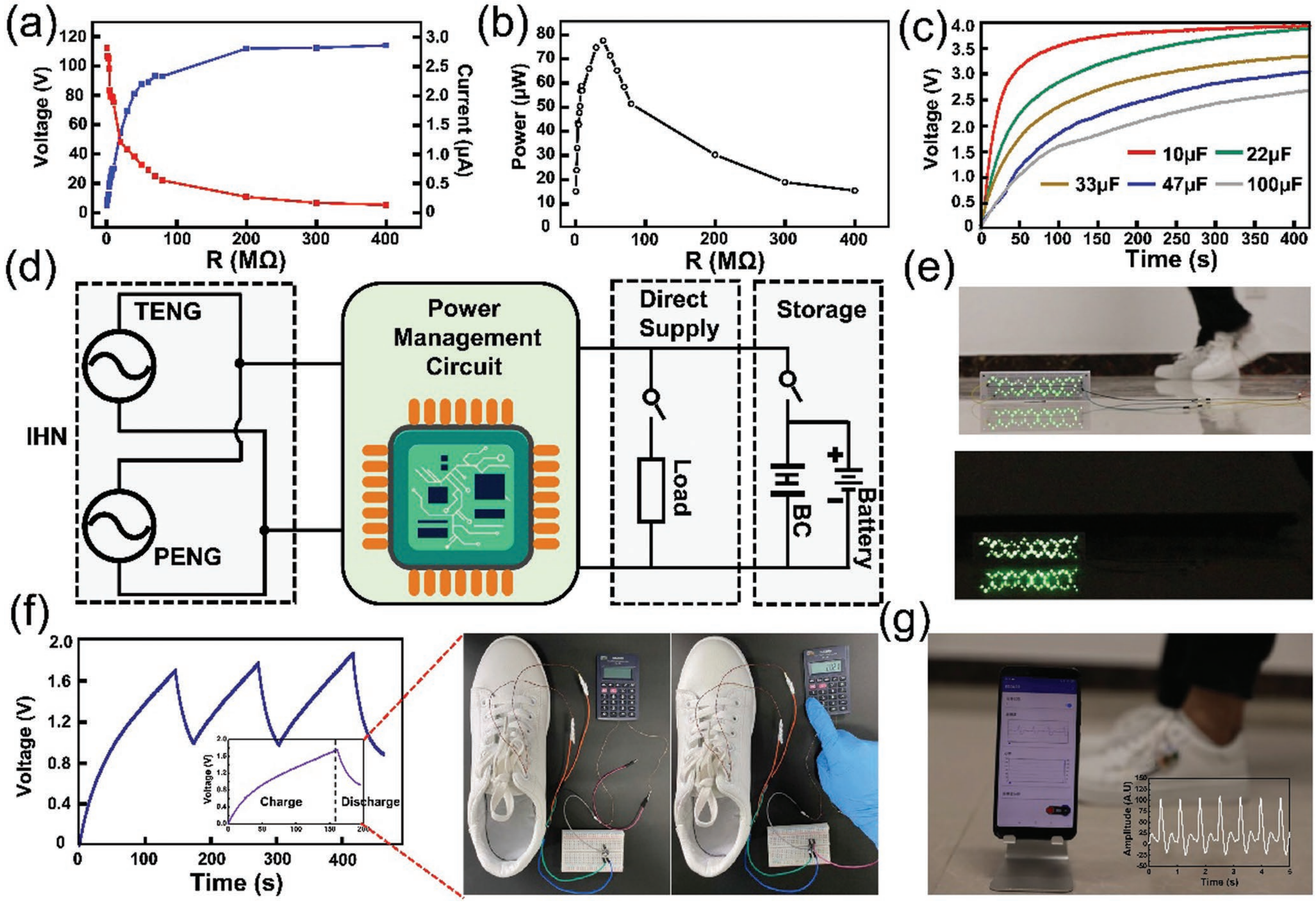

Figure 5. Power supply test and applications of IHN. a) Output voltage and current under the different external load resistances. b) Power curve under the different external load resistances. c) Charging capacity of the IHN under different specifications of capacitors. d) Schematic diagram of the IHN direct energy supply and energy storage. e) Graphs of the LEDs driven by the IHN. f) Energy curve and the device photos of the calculator powered by IHN. g) Display diagram of the dorsalis pedis artery monitoring system.

calculator is selected to evaluate the power supply capacity of IHN. The result is briefly in Figure 5f, the IHN charges a 47 μF capacitor from 0 to 1.7 V in 150 s, which can drive the calculator to run for 25 seconds and can perform about two simple mathematical calculations. To clarify the contribution of the TENG and the PENG in load power supply, the power densities of the two parts under different external loads were measured. As shown in Figure S6a,b (Supporting Information), a maximum power density of 0.28 $\mu W\ cm^{-2}$ was achieved by the TENG when the load resistance was 30 MΩ. Similarly, when the external resistance is 40 MΩ, the peak power density value of PENG reaches ≈0.36 $\mu W\ cm^{-2}$ (Figure S6c,d, Supporting Information). This shows that PENG provides greater power density than TENG but has a greater internal impedance.

Finally, we designed a self-powered dorsalis pedis artery monitoring system (SAMS) based on IHN (Figure 5g). The SAMS developed mainly includes an IHN sensor, a PVDF pulse sensor, and an integrated circuit board (Figure S7a, Supporting Information). Among them, the pulse sensor made of piezoelectric material is located on the inner side of the "tongue," and it is a self-powered device like the IHN. Additionally, the integrated circuit board consists of the signal processor, radio frequency transmitter, and power supply management circuits. In this system, the pulse sensor converts the blood pressure vibration in the dorsal artery of the foot into electrical signals, which are used to monitor the physiological information carried. The IHN acts as an energy harvester to collect the energy generated by the pedals. In particular, we have formulated a set of energy management strategies, where IHN and lithium-ion batteries provide energy for each module in the entire system. When the system is working, the energy is first supplied by the lithium-ion battery, and the energy captured by the IHN is stored in a large capacitor. Once the energy storage in the capacitor reaches a preset high threshold, the capacitor replaces the battery for energy supply. When the energy in the capacitor drops to a preset low threshold, it is powered by the battery again. The circuit diagram of this system is described in Figure S7b (Supporting Information). In the experiment, the pulse sensor successfully collected the pulse signal and sent it to the mobile phone APP by the wireless transmitter module (Video S4, Supporting Information). This strategy can effectively extend the service life of the SAMS and battery, and maximize the advantages of the IHN. The dorsal foot artery can reflect diseases such as arterial occlusive sclerosis of the lower extremities and diabetes, while the clinical dorsal foot artery monitoring system has many problems such as large size, high price, and the need for professional doctors. Therefore, the SAMS developed based on the IHN has great potential in the field of long-term medical monitoring and intelligent analysis.

3. Conclusion

In summary, an insole hybrid nanogenerator (IHN) with a TENG and a PENG has been developed to make a self-powered dorsalis pedis artery monitoring system. The TENG with a sandwich structure and the PENG with an arch structure ensure the stability of the output, and the design of the support and packaging guarantees its durability to adapt to a variety of application environments. The subtle structure enables the IHN not only to be adapted to collect mechanical energy in a variety of motion states, but also to identify human gait information. Besides, it reaches a 150 V open-circuit voltage and 4.5 V short circuit current from jumping and obtains the maximum output power of 77 μW under a 40 MΩ load during stepping. Superior energy harvesting capabilities make it easy to light up LEDs and drive small electronic devices such as calculators. Moreover, a SAMS based on the IHN was developed to monitor the physiological state of patients with lower extremity arteries or athletes. The integrated energy supply and sensing show that SAMS has great potential in long-term medical monitoring and health early warning.

4. Experimental Section

Fabrication of the TENG: The TENG was located on the forefoot of the IHN. First, two sponge insoles (the thickness of each layer was 5 mm) of the same size were cut by a laser cutting equipment (VOIERN, WER1080). Then multiple through-holes with a diameter of 2 cm were cut on the sponge insole. The first layer of sponge cut nine through-holes and the second layer of sponge cut eight through-holes. The through-holes of the two layers of sponges did not coincide, so as not to affect the comfort of wearing. According to the sandwich structure of sponge-Al-sponge, the three were bonded together with 3M tape. The outer side of the sponge was attached by PEFE. PTFE-Al-PTFE was separated by two layers of sponge and bonded with 3M tape. Then attached Cu electrode (0.15 mm thickness) on the back of PTFE. Because the sponge was processed with many through-holes, The Al and PTFE on both sides of the sponge contacted in the through-holes when the foot stepped on the IHN, forming the vertical contact and separation mode TENG. Finally, PE film and cloth were used to package the whole insole.

Fabrication of the PENG: The PENG was located on the heel of the IHN. PENG used commercially available 110 μm thick PVDF film as the piezoelectric material, and the size of PVDF was 1 cm × 5 cm strip shape. The lower surface of PVDF was bonded with a 2 cm × 7 cm arched Kapton film (0.1 mm thickness) through glass glue, and the upper surface of PVDF was covered with a layer of PE film (0.015 mm thickness). The arched Kapton film was made by hot pressing of a mold, and the arch height was 1 cm. The finished arched PENG was placed at room temperature for 12 h, and waited until the glass glue was completely solidified. Finally, part of the sponge at the heel of the insole was cut off and embedded PENG into the sponge.

Fabrication and Circuit Design of the SAMS: The dorsal foot artery sensor was also essentially a PENG. The commercially available 110 μm thick PVDF film was cut into a size of 2 cm × 1 cm, and then PTFE and Kapton films were used to encapsulate the PVDF device. When packaged, to drain the internal air, glass glue was used to bond, which could improve the durability of the sensor and the stability of the sensing signal. The IHN device was consistent with the previous description. It was made up of TENG and PENG through a sponge compound and was finally packaged with PE film and cotton cloth.

The pulse signal processor used a commercial HK2000 piezoelectric pulse sensor module, which had a Bluetooth transmission function. To realize that the energy generated by the IHN was applied to SAMS, an energy management circuit was designed based on the energy management chip LTC3331 (Figure S7b, Supporting Information). The energy of the IHN was stored in a capacitor of 22 μF through the LTC3331. Through the external circuit setting, the high and low thresholds of the capacitor voltage were preset to 10 and 5 V, respectively. When the energy in the capacitor was <5 V, SAMS was powered by the battery. However, when the energy in the capacitor was higher than 10 V, the capacitor started to supply power from the battery until the voltage dropped to the 5 V threshold. The pulse signal processor, energy management circuit, and battery were integrated with tape and silica gel, and the output ports of the IHN and pulse sensor were reserved, as shown in Figure S7a (Supporting Information).

Electrical Measurement: In Figure S2 (Supporting Information), a linear motor was used to study the composite output relationship between TENG and PENG in parallel. The linear motor used a frequency of 1.25 Hz to apply pressure to the IHN regularly, when the bidirectional acceleration of the motor was 1.5 m s^{-2} and the distance to press down was 5 mm. After TENG and PENG were connected in parallel, a digital oscilloscope and electrometer were used for electrical characterization. The same method was executed in the frequency response test (Figure S3, Supporting Information), the condition became 0.8–2.4 Hz, and the corresponding bidirectional acceleration was 0.1, 0.5, 3.5, 8, and 42 m s^{-2}, respectively. Similarly, the fatigue test used the same measurement system to collect data. The measurement system consisted of a linear motor with an acrylic plate, an oscilloscope, and an IHN, as shown in Figure S4a (Supporting Information).

The experiments involving human subjects had been performed with the full, informed consent of the volunteer, who was also a co-author of the manuscript. All experiments were approved by the Committee on Ethics of Beijing Institute of Nanoenergy and Nanosystems (A-2020009).

Supporting Information

Supporting Information is available from the Wiley Online Library or from the author.

Acknowledgements

M.D. and Y.C. contributed equally to this work. This work was supported by the National Natural Science Foundation of China (61875015, T2125003, 32101117), the Strategic Priority Research Program of the Chinese Academy of Sciences (XDA16021101), the Beijing Natural Science Foundation (JQ20038, L212010), and the Fundamental Research Funds for the Central Universities.

Conflict of Interest

The authors declare no conflict of interest.

Data Availability Statement

The data that support the findings of this study are available from the corresponding author upon reasonable request.

Keywords

biosensors, hybrid nanogenerators, PENG, TNEG, wearable devices

Received: October 9, 2021
Revised: January 6, 2022
Published online:

[1] a) M. C. Silva, V. J. P. Amorim, S. P. Ribeiro, R. A. R. Oliveira, *Sensors* **2019**, *19*, 4417; b) F. Wu, T. Y. Wu, M. R. Yuce, *Sensors-Basel* **2019**, *19*, 21.
[2] K. Mohammad, T. Tekeste, B. Mohammad, H. Saleh, M. Qurran, *Microelectron. J.* **2019**, *93*, 104634.
[3] a) S. S. Kwak, H. J. Yoon, S. W. Kim, *Adv. Funct. Mater.* **2019**, *29*, 2; b) X. H. Ren, X. Y. Xiang, H. F. Yin, Y. Tang, H. D. Yuan, *Nanotechnology* **2021**, *32*, 315404; c) X. Pu, M. M. Liu, X. Y. Chen, J. M. Sun, C. H. Du, Y. Zhang, J. Y. Zhai, W. G. Hu, Z. L. Wang, *Sci. Adv.* **2017**, *3*, 1700015.
[4] a) D. J. Jiang, H. Ouyang, B. J. Shi, Y. Zou, P. C. Tan, X. C. Qu, S. Y. Chao, Y. Xi, C. C. Zhao, Y. B. Fan, Z. Li, *Infomat* **2020**, *2*, 1191; b) X. D. Zhong, Y. Yang, X. Wang, Z. L. Wang, *Nano Energy* **2015**, *13*, 771; c) H. Q. Feng, Y. Bai, L. Qiao, Z. Li, E. G. Wang, S. Y. Chao, X. C. Qu, Y. Cao, Z. Liu, X. Han, R. Z. Luo, Y. Z. Shan, Z. Li, *Small* **2021**, *17*, 2101430.
[5] a) S. K. Karan, R. Bera, S. Paria, A. K. Das, S. Maiti, A. Maitra, B. B. Khatua, *Adv. Energy Mater.* **2016**, *6*, 1601016; b) M. Zhang, T. Gao, J. S. Wang, J. J. Liao, Y. Q. Qiu, Q. Yang, H. Xue, Z. Shi, Y. Zhao, Z. X. Xiong, L. F. Chen, *Nano Energy* **2015**, *13*, 298; c) S. Azimi, A. Golabchi, A. Nekookar, S. Rabbani, M. H. Amiri, K. Asadi, M. M. Abolhasani, *Nano Energy* **2021**, *83*, 105781.
[6] a) L. Y. Ma, R. H. Wu, A. Patil, J. Yi, D. Liu, X. W. Fan, F. F. Sheng, Y. F. Zhang, S. Liu, S. Shen, J. Wang, Z. L. Wang, *Adv. Funct. Mater.* **2021**, *31*, 2102963; b) C. Y. Chen, L. J. Chen, Z. Y. Wu, H. Y. Guo, W. D. Yu, Z. Q. Du, Z. L. Wang, *Mater. Today* **2020**, *32*, 84; c) Z. H. Zhou, L. Weng, T. Tat, A. Libanori, Z. M. Lin, L. J. Ge, J. Yang, J. Chen, *ACS Nano* **2020**, *14*, 14126.
[7] I. Galili, D. Kaplan, Y. Lehavi, *Am. J. Phys.* **2006**, *74*, 337.
[8] S. Lee, R. Hinchet, Y. Lee, Y. Yang, Z. H. Lin, G. Ardila, L. Montes, M. Mouis, Z. L. Wang, *Adv. Funct. Mater.* **2014**, *24*, 1163.
[9] C. Covaci, A. Gontean, *Sensors-Basel* **2020**, *20*, 3512.
[10] a) J. Song, B. Yang, W. Zeng, Z. H. Peng, S. P. Lin, J. Li, X. M. Tao, *Adv. Mater. Technol.* **2018**, *3*, 1704022; b) A. S. Dahiya, F. Morini, S. Boubenia, K. Nadaud, D. Alquier, G. Poulin-Vittrant, *Adv. Mater. Technol.* **2018**, *3*, 1700249.
[11] W. B. Ding, A. C. Wang, C. S. Wu, H. Y. Guo, Z. L. Wang, *Adv. Mater. Technol.* **2019**, *4*, 1800487.
[12] a) T. Chen, Q. F. Shi, M. L. Zhu, T. Y. Y. He, L. N. Sun, L. Yang, C. Lee, *ACS Nano* **2018**, *12*, 11561; b) L. Liu, Q. F. Shi, Z. D. Sun, C. K. Lee, *Nano Energy* **2021**, *86*, 106154; c) Q. F. Shi, C. K. Lee, *Adv. Sci.* **2019**, *6*, 1900617.
[13] a) Q. Zhang, Z. Zhang, Q. J. Liang, F. F. Gao, F. Yi, M. Y. Ma, Q. L. Liao, Z. Kang, Y. Zhang, *Nano Energy* **2019**, *55*, 151; b) T. C. Zhao, M. Y. Xu, X. Xiao, Y. Ma, Z. Li, Z. L. Wang, *Nano Energy* **2021**, *88*, 106199; c) Z. L. Wang, T. Jiang, L. Xu, *Nano Energy* **2017**, *39*, 9.
[14] S. Choi, S. Cho, Y. Yun, S. Jang, J. H. Choi, Y. Ra, M. La, S. J. Park, D. Choi, *Adv. Mater. Technol.* **2020**, *5*, 2000003.
[15] a) Z. Li, G. A. Zhu, R. S. Yang, A. C. Wang, Z. L. Wang, *Adv. Mater.* **2010**, *22*, 2534; b) R. Yang, Y. Qin, C. Li, G. Zhu, Z. L. Wang, *Nano Lett.* **2009**, *9*, 1201.
[16] a) B. J. Shi, Z. Liu, Q. Zheng, J. P. Meng, H. Ouyang, Y. Zou, D. J. Jiang, X. C. Qu, M. Yu, L. M. Zhao, Y. B. Fan, Z. L. Wang, Z. Li, *ACS Nano* **2019**, *13*, 6017; b) K. W. Zhang, Z. L. Wang, Y. Yang, *ACS Nano* **2016**, *10*, 4728.
[17] H. Ouyang, Z. Liu, N. Li, B. J. Shi, Y. Zou, F. Xie, Y. Ma, Z. Li, H. Li, Q. Zheng, X. C. Qu, Y. B. Fan, Z. L. Wang, H. Zhang, Z. Li, *Nat. Commun.* **2019**, *10*, 1821.
[18] a) Q. Zheng, B. J. Shi, F. R. Fan, X. X. Wang, L. Yan, W. W. Yuan, S. H. Wang, H. Liu, Z. Li, Z. L. Wang, *Adv. Mater.* **2014**, *26*, 5851; b) S. Wang, H. L. Tai, B. H. Liu, Z. H. Duan, Z. Yuan, H. Pan, Y. J. Su, G. Z. Xie, X. S. Du, Y. D. Jiang, *Nano Energy* **2019**, *58*, 312.
[19] M. G. Abdelmageed, A. M. R. F. El-Bab, A. A. Abouelsoud, *Microelectron. J.* **2019**, *86*, 105.
[20] a) K. Tao, H. P. Yi, Y. Yang, L. H. Tang, Z. S. Yang, J. Wu, H. L. Chang, W. Z. Yuan, *Microsyst. Nanoeng.* **2020**, *6*, 56; b) Y. J. Han, Y. F. Han, X. P. Zhang, L. Li, C. W. Zhang, J. H. Liu, G. Lu, H. D. Yu, W. Huang, *ACS Appl. Mater. Interfaces* **2020**, *12*, 16442.
[21] A. Toprak, O. Tigli, *Appl. Phys. Rev.* **2014**, *1*, 031104.
[22] a) H. H. Singh, N. Khare, *Nano Energy* **2018**, *51*, 216; b) H. H. Singh, S. Singh, N. Khare, *Polym. Adv. Technol.* **2018**, *29*, 143.
[23] a) S. M. Kim, *Eur Phys J Plus* **2018**, *133*, 1; b) F. Xing, Y. Jie, X. Cao, T. Li, N. Wang, *Nano Energy* **2017**, *42*, 138; c) Z. L. Wang, *ACS Nano* **2013**, *7*, 9533.
[24] a) Z. L. Wang, *Mater. Today* **2017**, *20*, 74; b) C. S. Wu, A. C. Wang, W. B. Ding, H. Y. Guo, Z. L. Wang, *Adv. Energy Mater.* **2019**, *9*, 1802906.

